Environmental Science & Technology LETTERS

pubs.acs.org/journal/estlcu

Letter

Real-Time Measurements of Botanical Disinfectant Emissions, Transformations, and Multiphase Inhalation Exposures in Buildings

Jinglin Jiang, Xiaosu Ding, Antonios Tasoglou, Heinz Huber, Amisha D. Shah, Nusrat Jung,* and Brandon E. Boor*

Cite This: *Environ. Sci. Technol. Lett.* 2021, 8, 558–566

Read Online

ACCESS | Metrics & More | Article Recommendations | Supporting Information

ABSTRACT: Thymol-based botanical disinfectants have emerged as natural alternatives to traditional chemical disinfectants given their effectiveness as antimicrobial pesticides and ability to inactivate SARS-CoV-2. This study investigates the impact of botanical disinfectants on indoor air chemistry and human exposure. Controlled surface disinfection experiments were conducted in a mechanically ventilated zero-energy tiny house laboratory. Volatile organic compounds (VOCs) and aerosol size distributions were measured in real-time (1 Hz) with a proton transfer reaction time-of-flight mass spectrometer and a high-resolution electrical low-pressure impactor, respectively. Botanical disinfectant spray and wipe products drove sudden changes in the chemical composition of indoor air. Mixing ratios of monoterpenes ($C_{10}H_{16}$) and monoterpenoids ($C_{10}H_{14}O$, $C_{10}H_{16}O$, $C_{10}H_{18}O$, and $C_{10}H_{20}O$) increased suddenly during the disinfection events (10^{-1} to 10^{2} ppb) and exhibited volatility-dependent temporal emission profiles. VOC emission factors ranged from 10^{0} to 10^{4} $\mu g\ g^{-1}$, and thymol intake fractions ranged from 6 to 7×10^{3} ppm. Rapid new particle formation events were observed due to ozonolysis of monoterpenes and monoterpenoids, increasing sub-100 nm particle number concentrations by 10^{4} to 10^{5} cm^{-3}. Botanical disinfectant sprays initiated multiphase inhalation exposure to VOCs, secondary organic aerosol, and sub-10 μm droplets, with large deposited doses in each respiratory tract region associated with the latter two.

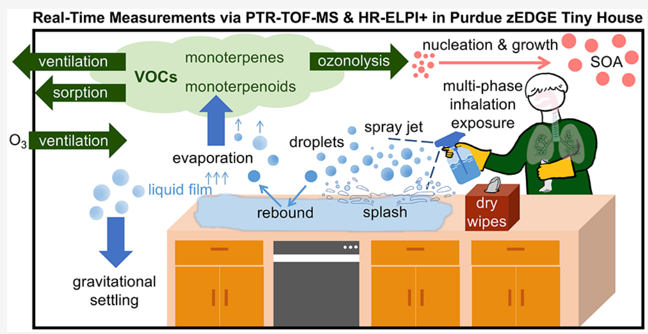

INTRODUCTION

The COVID-19 pandemic has led to increased levels of chemical disinfection of high-touch indoor surfaces in buildings to minimize fomite transmission.[1−3] Antimicrobial pesticides proven to be effective in inactivating SARS-CoV-2 are summarized in the U.S. Environmental Protection Agency List N: Disinfectants for Coronavirus.[4] The most widely used active ingredients among disinfectant products included in List N can be classified as (1) quaternary ammonium salts, e.g., benzalkonium chlorides; (2) oxidizers, e.g., sodium hypochlorite and hydrogen peroxide; and (3) alcohols, e.g., ethanol and isopropyl alcohol.[4,5] The ubiquitous use of these compounds in buildings has raised concern given their adverse impact on indoor environments and human health.[5−12]

Botanical or essential oil-based disinfectants have emerged as natural and green alternatives to traditional chemical disinfectants. Many of these products incorporate thymol ($C_{10}H_{14}O$) as the active ingredient. Thymol has been shown to be effective as an antioxidant[13,14] and antimicrobial.[15−18] Thymol has been used in wound dressings,[19,20] in-feed antibiotics,[21] and antibacterial products[22−28] as it can disrupt bacterial cell membrane integrity and initiate cell death.[29] Thymol-based oral rinses have shown >99.9% efficacy in inactivating SARS-CoV-2 surrogates.[30,31] Thymol-based disinfectants are included in List N.[4]

Routine use of thymol-based botanical disinfectants in buildings has important implications for indoor chemistry as products containing essential oils are expected to emit a variety of monoterpenes and monoterpenoids[32−34] that can be oxidized by ozone (O_3) to form secondary organic aerosol (SOA).[35−37] However, little is known regarding how botanical disinfectants alter the chemical composition of indoor air. The objective of this study is to characterize botanical disinfectant emissions, transformations, and exposures through real-time (1 Hz) measurements of volatile organic compounds (VOCs) with a proton transfer reaction time-of-flight mass spectrometer (PTR-TOF-MS) and aerosols with a high-resolution electrical low-pressure impactor (HR-ELPI+).

Received: May 24, 2021
Revised: June 3, 2021
Accepted: June 3, 2021
Published: June 9, 2021

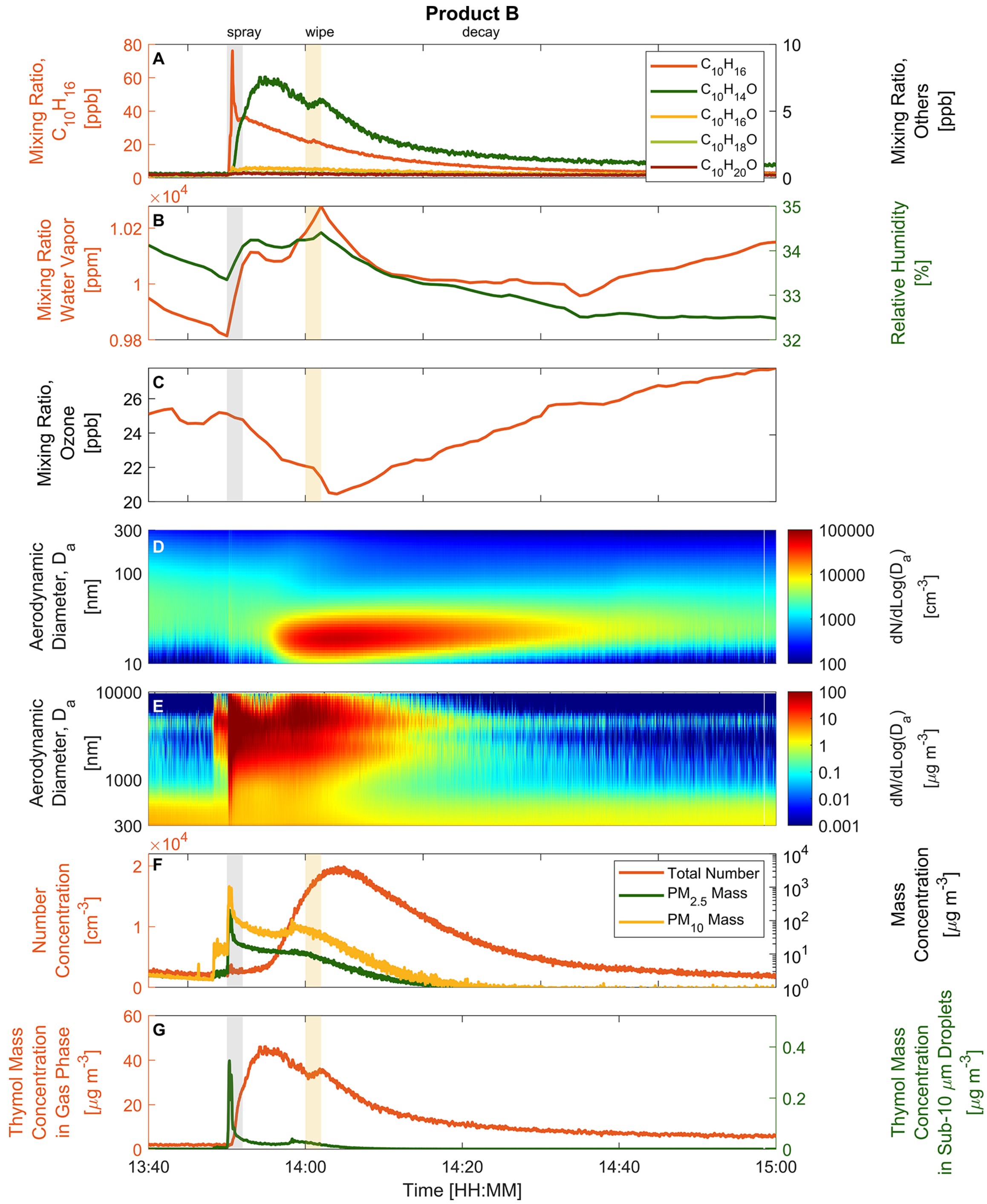

Figure 1. Time series for botanical disinfection experiment B2 using spray product B (thymol, 0.05 wt %). (A) Mixing ratio of $C_{10}H_{16}$ (orange line, left *y*-axis), $C_{10}H_{14}O$ (dark green line, right *y*-axis), $C_{10}H_{16}O$ (yellow line, right *y*-axis), $C_{10}H_{18}O$ (light green line, right *y*-axis), and $C_{10}H_{20}O$ (dark red line, right *y*-axis). (B) Mixing ratio of water vapor (orange line, left *y*-axis) and indoor relative humidity (dark green line, right *y*-axis). (C) Mixing ratio of ozone (orange line). (D) Aerosol number size distribution at D_a values from 10 to 300 nm. (E) Aerosol mass size distribution at D_a values from 300 to 10000 nm. (F) Size-integrated aerosol number concentration at D_a values from 10 to 10000 nm (orange line, left *y*-axis) and size-integrated mass concentration at D_a values from 10 to 2500 nm ($PM_{2.5}$, dark green line, right *y*-axis) and from 10 to 10000 nm (PM_{10}, yellow line, right *y*-axis). (G) Thymol mass concentration in the gas phase (orange line, left *y*-axis) and sub-10 μm droplets (dark green line, right *y*-axis). Gray shading represents the period of disinfectant application, and light yellow shading represents the period of dry wiping the disinfectant residue off the glass slides. The dry wiping process likely enhances mass transfer from the liquid disinfectant on the glass panels and dry wipes, which can explain the slight increase in VOC mixing ratios during this period.

■ MATERIALS AND METHODS

The measurement campaign was conducted in a residential architectural engineering laboratory, the Purdue zero Energy Design Guidance for Engineers (zEDGE) Tiny House (volume of 60.35 m^3) (Figures S1 and S2). The zEDGE Tiny House is configured with a powered ventilator with a MERV 16 filter that maintained an outdoor air exchange rate (AER) of 3 h^{-1}. Mixing ratios of VOCs were measured with a PTR-TOF-MS

https://doi.org/10.1021/acs.estlett.1c00390
Environ. Sci. Technol. Lett. 2021, 8, 558−566

(PTR-TOF 4000, Ionicon Analytik Ges.m.b.H., Innsbruck, Austria). Particle size distributions from 6 to 10000 nm in aerodynamic diameter (D_a) were measured with a HR-ELPI+ (Dekati Ltd., Kangasala, Finland).[38−42] Six thymol-based botanical disinfectants (spray, A−E; wet wipe, G) and one non-thymol-based botanical disinfectant (spray, F) were tested (Table S1). Three 80 min emission experiments (Figure S3) were completed for each of the seven disinfectants (e.g., A1−A3), for a total of 21 experiments. The disinfectant was applied to two glass panels on the kitchen countertop.

RESULTS AND DISCUSSION

Temporal Variations in VOC Concentrations during Indoor Botanical Disinfection Events. The use of spray- and wipe-based botanical disinfectants in buildings results in sudden changes in the chemical composition of indoor air. Figure 1 is a representative example of the temporal VOC emission profiles associated with a thymol-based botanical disinfectant spray. Immediately after indoor surface disinfection with product B, mixing ratios for monoterpenes ($C_{10}H_{16}$, detected at m/z 137 and 81, possibly D-limonene, α-pinene, β-pinene, or γ-terpinene) increased rapidly. A peak mixing ratio of 76.11 ppb was reached within seconds of application, 40-fold greater than background levels in the zEDGE Tiny House. This suggests that botanical disinfectants can be important episodic sources of monoterpenes during routine building disinfection.

The emission profile of the disinfectant itself, thymol ($C_{10}H_{14}O$, m/z 151), was distinctly different from that of the monoterpenes (Figure 1A). The thymol mixing ratio gradually increased over time, reaching a peak (7.56 ppb) nearly 4 min after application of the botanical disinfectant. The observed variations in the emission profiles between thymol and monoterpenes are likely due to their different enthalpies of vaporization, $\Delta_{vap}H°$. A higher $\Delta_{vap}H°$ indicates a lower volatility, expressed as the saturation concentration, C^* (Table S3).[43,44] With a higher $\Delta_{vap}H°$ and a lower C^*, thymol evaporates more slowly than various monoterpenes. The thymol emission profiles for the wet wipe (G) were similar to those for the sprays (A−E); however, thymol mixing ratios were the lowest among the thymol-containing products tested.

The PTR-TOF-MS measurements revealed the presence of several additional monoterpenoids in the botanical disinfectant emissions, including $C_{10}H_{16}O$ (m/z 153, possibly camphor or citral), $C_{10}H_{18}O$ (m/z 155, possibly linalool, α-terpineol, eucalyptol, citronellal, or terpinen-4-ol), and $C_{10}H_{20}O$ (m/z 157, possibly decanal, citronellol, or menthol). Such compounds are found in various essential oils,[45−47] some of which were listed on the product label (Table S1). Peak mixing ratios typically remained below 10 ppb. As illustrated in Figure S13, the temporal emission profiles for $C_{10}H_{16}O$ and $C_{10}H_{18}O$ are more like that of the monoterpenes, likely due to their similar C^* values. Among the six thymol-based botanical disinfectants evaluated in this study (A−E and G), none were found without the coexistence of monoterpenes and other monoterpenoids due to their inclusion in essential oils. For five of the six products, monoterpenes were associated with the highest peak mixing ratios, often >50 ppb, among the identified VOCs. However, for product E, thymol mixing ratios exceeded those of monoterpenes, likely due to the inclusion of thymol at 0.23 wt %.

Mixing ratios of monoterpenes, thymol, and other monoterpenoids remained elevated during the 10 min contact time of the botanical disinfectant on the surface (Figure 1A). Of the products tested, a majority specify a 10 min contact time for surface disinfection with thymol. This extends the effective volatilization period for VOCs included in the liquid disinfectant solution, thereby maintaining elevated indoor concentrations of volatile species. The removal of the liquid surface film of disinfectant with a dry wipe initiates the nearly exponential decay in mixing ratios due to VOC loss via ventilation and surface sorption.

Temporal Variations in Aerosol Size Distributions and Concentrations during Indoor Botanical Disinfection Events. Real-time aerosol measurements with a HR-ELPI+ during the botanical disinfection experiments revealed two distinct aerosol generation events: (1) new particle formation (NPF) due to the ozonolysis of selected VOCs released by the disinfectants and (2) disinfectant droplet formation during the spray process (for products A−F). The pulse release of monoterpenes and monoterpenoids was associated with a decrease in O_3 mixing ratios from 25 to 20 ppb (Figure 1C). Depletion of O_3 was observed across most of the disinfection events. Various monoterpenes and monoterpenoids can be oxidized by O_3 to more oxygenated and less volatile products that can initiate the formation of indoor SOA.[48] Indoor NPF events were observed during six of the 21 botanical surface disinfection experiments (Table S5); an example is shown in panels D and F of Figure 1. VOC, O_3, and SOA concentrations for each NPF event are listed in Table S6.

For products B and D, particle number (PN) concentrations began to steadily increase approximately 5 min after application of the thymol-based botanical disinfectant (B2 in Figure 1F, B3 in Figure S10F, and D1 in Figure S14F). Peak PN concentrations were reached several minutes after dry wiping the disinfectant film from the glass panels. Product F, a non-thymol-based disinfectant, exhibited a different temporal profile in PN concentrations, with levels rising sharply 2−3 min after disinfectant application and peaking several minutes before the dry wipe (Figures S20F−S22F). Higher sub-100 nm PN concentrations were obtained during the indoor NPF events with the non-thymol-based disinfectant [e.g., F2 peak, 4.45×10^5 cm^{-3} (Figure S21F)] as compared to the two thymol-based botanical disinfectants [e.g., B2 peak, 1.96×10^4 cm^{-3} (Figure 1F)], likely due to greater emissions of $C_{10}H_{16}$ and $C_{10}H_{16}O$ from the former (Table S5). Production of sub-100 nm particles on the order of 10^4−10^5 cm^{-3} demonstrates the strong SOA-forming potential of botanical disinfectants used in the presence of O_3 in mechanically ventilated buildings undergoing routine surface disinfection. Among the observed NPF events, the newly formed particles grew quickly, at D_a values from <10 to >40 nm in several minutes (e.g., Figure 1D and Figure S21D).

The concurrent release of a variety of VOCs that have high reactivities with O_3 (Table S3) suggests that the indoor NPF events were initiated by the ozonolysis of both the emitted monoterpenes ($C_{10}H_{16}$) and monoterpenoids ($C_{10}H_{14}O$, $C_{10}H_{16}O$, $C_{10}H_{18}O$, and $C_{10}H_{20}O$). The former likely played a leading role in the production of highly oxygenated organic molecules (HOMs)[49−52] given the high mixing ratios observed (Table S5). While SOA production due to monoterpene ozonolysis has been well studied,[36,37,53−56] comparatively less is known with regard to monoterpenoid ozonolysis. A few studies have observed SOA production due to the ozonolysis of $C_{10}H_{16}O$ and $C_{10}H_{18}O$ isomers,[37,57−62] while $C_{10}H_{14}O$ and $C_{10}H_{20}O$ isomers have not yet been evaluated. In addition to

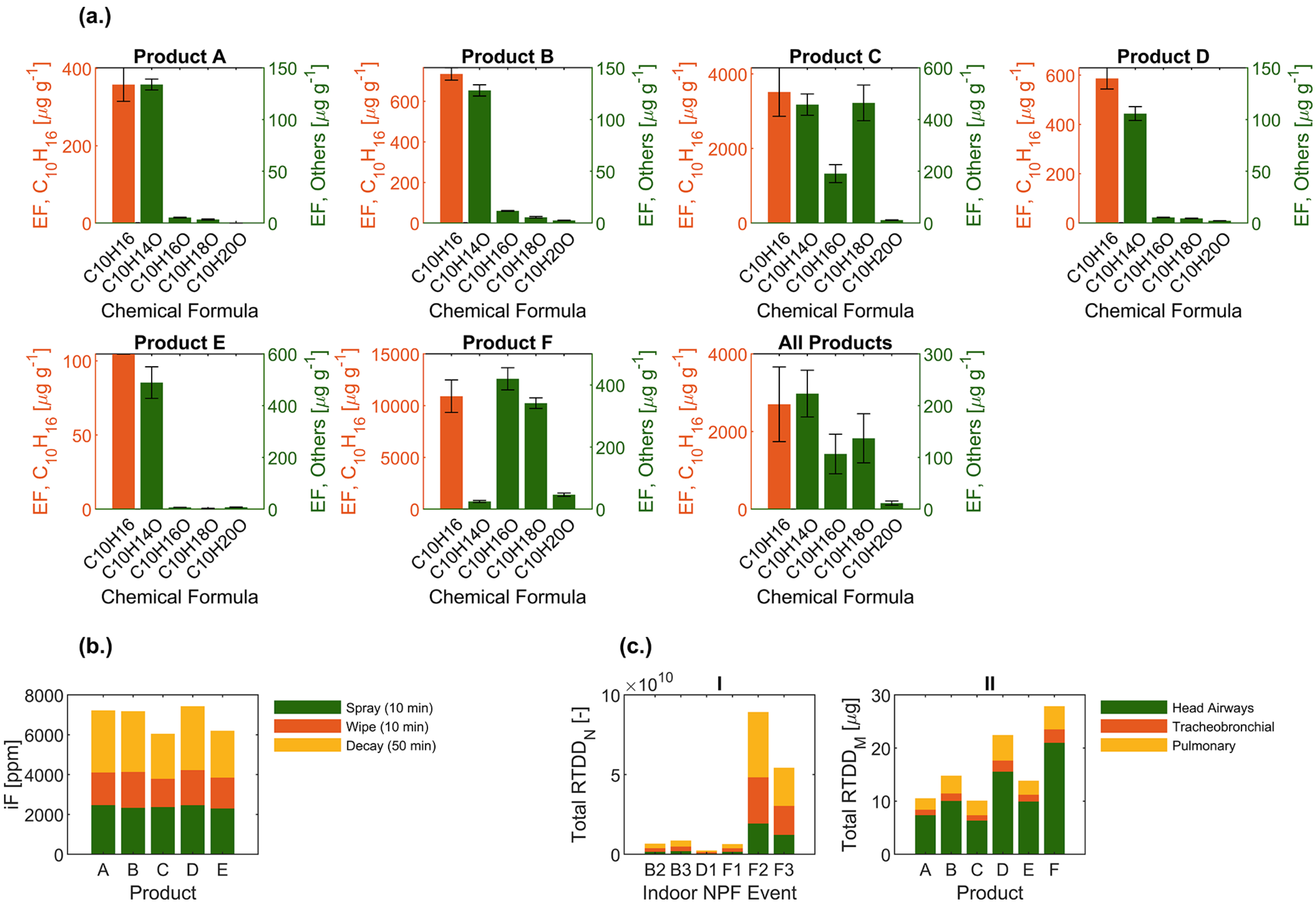

Figure 2. (a) Mean speciated emission factors (EFs) for $C_{10}H_{16}$ (left *y*-axis), $C_{10}H_{14}O$ (right *y*-axis), $C_{10}H_{16}O$ (right *y*-axis), $C_{10}H_{18}O$ (right *y*-axis), and $C_{10}H_{20}O$ (right *y*-axis) for botanical disinfectant products A−F (micrograms per gram). For subplots A−F, the error bars represent the standard deviation for triplicate experiments for each product. The bottom right subplot includes mean speciated EFs aggregated across all experiments for all spray products (A−F). The error bars represent the standard deviation across all experiments for all spray products (A−F). It should be noted that each of these values represents the sum of EFs of compounds with the same chemical formula as the PTR-TOF-MS is not able to separate isomers. (b) Thymol ($C_{10}H_{14}O$) inhalation intake fraction (iF) for the thymol-based botanical disinfectant spray products (A−E), partitioned into the spray period (10 min, dark green), dry wipe period (10 min, dark red), and decay period (50 min, yellow). (c) (I) Cumulative size-integrated (D_a = 10−10000 nm) number respiratory tract deposited dose ($RTDD_N$) for inhaled aerosols to the head airways (dark green), tracheobronchial region (dark red), and pulmonary region (yellow) for the six experiments in which new particle formation (NPF) events were observed (B2, B3, D1, and F1−F3). (II) Cumulative size-integrated (D_a = 10−10000 nm) mass respiratory tract deposited dose ($RTDD_M$) for inhaled aerosols to the head airways (dark green), tracheobronchial region (dark red), and pulmonary region (yellow) for botanical disinfectant products (A−F). For panels b and c(II), the values represent the means of triplicate experiments for each product. RTDDs were calculated for an adult engaged in light activity (e.g., cleaning) based on a 70 min exposure period, starting from the application of the disinfectant.

HOMs produced by the ozonolysis of monoterpenes and monoterpenoids, it is likely that human-emitted ammonia (NH_3)[63,64] (via the researcher applying the disinfectant) and outdoor-to-indoor transported sulfuric acid (H_2SO_4)[65−68] (via the powered ventilator) participated in the initial steps of particle nucleation and growth. Given a per-person NH_3 emission factor[63] of 0.6 mg h^{-1} person^{-1}, a researcher in the zEDGE Tiny House for 10 min can increase indoor NH_3 mixing ratios by ∼1.9 ppb. Outdoor H_2SO_4 measurements in Indiana have reported concentrations in the range of 10^6−10^7 molecules cm^{-3}.[69] Prior observations[65,70] of atmospheric NPF events at similar or lower H_2SO_4 and NH_3 concentrations would suggest that both species contributed to the observed indoor NPF events.

The HR-ELPI+ measurements revealed the formation of coarse mode liquid droplets during the application of the botanical disinfectant sprays. As illustrated in panels E and F of Figure 1, particle mass concentrations at D_a values from 1 to 10 μm sharply increased at the inception of the spray event. Peak PM_{10} and $PM_{2.5}$ mass concentrations were on the order of 10^2−10^3 and 10^1−10^2 μg m^{-3}, respectively, across the disinfection events (Table S5). Thus, botanical disinfectant sprays are important episodic indoor sources of coarse mode particles. The observed formation of sub-10 μm droplets during botanical disinfection events can be attributed to three physical processes: (1) direct emissions of sub- and super-10 μm droplets from the spray jet,[71,72] (2) impaction of super-10 μm droplets onto the glass panels, followed by droplet rebound or initiation of splashes that can release smaller droplets into the air;[71,73] and (3) shrinkage of super-10 μm droplets due to evaporation.[71,73,74] The rapid decrease in PM_{10} concentrations after the spray event is due to droplet evaporation, gravitational settling, and ventilation. The former can explain the concurrent increase in water vapor mixing ratios (Figure 1B).

There exist two pathways by which monoterpenes and monoterpenoids included in the liquid disinfectant solutions can be released into the air: (1) evaporation from the liquid film on the surface to be disinfected and (2) evaporation from the sub- and super-10 μm droplets (for products A−F). The disinfectant itself, thymol, can therefore exist in two phases concurrently. Figure 1G illustrates the measured mass concentration of thymol in the gas phase and that contained in the sub-10 μm droplets, estimated on the basis of the measured PM_{10} mass concentrations and initial thymol weight percentage. The distribution of thymol between the two phases was temporally variant, with a spike in the droplet phase occurring ∼4 min before the peak in the gas phase.

Botanical Disinfectant Emission Factors for VOCs and Sub-10 μm Droplets. Real-time measurements of the botanical disinfectant emissions via the PTR-TOF-MS and HR-ELPI+ enabled determination of emission factors (EFs) for VOCs (Figure 2a) and sub-10 μm droplets (Figure S27). EFs are a generalizable metric for quantifying the total amount of species emitted per unit of a product applied.[33,75] VOC EFs are reported as micrograms per gram, micrograms per milliliter, and micrograms per spray for products A−F and micrograms per wipe for product G (Table S7). Speciated EFs in micrograms per gram for sprays A−F are presented in Figure 2a. Thymol EFs for the nonpressurized sprays containing thymol at 0.05 wt % (A, B, and D) were similar, ranging from 106 to 134 $\mu g\ g^{-1}$. Thymol EFs scaled with the amount of thymol included in the disinfectant. The mean thymol EF for product E (0.23 wt %) was 489 $\mu g\ g^{-1}$, 3.6−4.6-fold greater than EFs for products containing 0.05 wt % thymol (A, B, and D; all for nonpressurized sprays). This agrees with the ratio of the thymol weight percentage (0.23 wt %/0.05 wt % = 4.6).

EFs varied among the monoterpenes and monoterpenoids released from the botanical disinfectants, with the following mean EFs aggregated across all spray products (A−F): $C_{10}H_{16}$, 2701 $\mu g\ g^{-1}$; $C_{10}H_{14}O$, 223.2 $\mu g\ g^{-1}$; $C_{10}H_{16}O$, 106.7 $\mu g\ g^{-1}$; $C_{10}H_{18}O$, 136.9 $\mu g\ g^{-1}$; $C_{10}H_{20}O$, 11.7 $\mu g\ g^{-1}$ (Figure 2a, bottom right subplot). Product F, a non-thymol-based disinfectant, had the highest EFs for $C_{10}H_{16}$, $C_{10}H_{16}O$, and $C_{10}H_{20}O$. Among the thymol-based sprays (A−E), product C had the highest EFs for $C_{10}H_{16}$, $C_{10}H_{16}O$, $C_{10}H_{18}O$, and $C_{10}H_{20}O$. EFs for sub-10 μm droplets ranged from 0.5 to 4.5 mg $spray^{-1}$, corresponding to emission rates from 0.5 to 2.4 mg s^{-1}, respectively (Figure S27).

For the spray products, the VOC EFs depend in part on the amount of each compound added to the liquid disinfectant solution and the compound's volatility. The former was given for only thymol. In the United States, manufacturers are required to disclose the weight percentage for only nonfunctional constituents included at >0.01 wt %, as per California's SB-258 Cleaning Product Right to Know Act of 2017.[76] Despite the inclusion of monoterpenes at <0.01 wt %, EFs were greater than that for thymol for all products with 0.05 wt % thymol due to the higher volatility of monoterpenes (e.g., the D-limonene C^* is 86-fold greater than the thymol C^*). Thus, policies regarding consumer products intended to be sprayed in indoor environments should consider not only the weight percentage of a particular ingredient but also the extent to which they can partition into the air. In this study, the EFs were determined for disinfectants applied to impermeable glass panels. It is expected that the VOC emission profiles and EFs would vary among different application surfaces, such as porous wood and fabric-covered furniture.

Human Exposure Implications of Botanical Disinfection Events in Buildings. The use of botanical disinfectants in mechanically ventilated residential buildings in the presence of O_3 initiates a temporally variant multiphase inhalation exposure scenario. As illustrated in Figure 1, one is first exposed to primary emissions of gas-phase monoterpenes and monoterpenoids and coarse mode liquid droplets of the disinfectant solution, followed by ozonolysis-initiated sub-100 nm SOA. Thymol inhalation intake fractions (iFs)[77−79] and aerosol respiratory tract deposited doses in number ($RTDD_N$s) and mass ($RTDD_M$s)[80−85] were determined to characterize human exposure to botanical disinfectant emissions at different breathing rates.[75−77] Panels b and c of Figure 2 present results for an adult engaged in light activity (e.g., cleaning)[86] (inhalation rate of 1.25 $m^3\ h^{-1}$). Results for other breathing rates, including a breathing rate adjusted exposure[87] scenario, are presented in Figure S29.

Thymol iFs ranged from 6 to 7 × 10^3 ppm among the five thymol-based disinfectant spray products, indicating that >0.6% of the thymol emitted into the gas phase can be inhaled during a disinfection event (Figure 2b). These values are within the range of previously reported iFs for different indoor emission sources.[78,88] One-third of the total inhalation intake occurred during the spray period when the thymol mixing ratio reached its peak (Figure 1A). The inhalation intake of thymol during the 50 min decay period was the greatest among the three periods, accounting for ∼40% of the total iF. Thus, one can inhale a significant amount of thymol after the liquid film of disinfectant is removed from a surface. The variability in the iFs among the spray, wipe, and decay periods demonstrates the utility of real-time indoor VOC exposure measurements with a PTR-TOF-MS.

Inhalation exposure to ozonolysis-initiated SOA resulted in $RTDD_N$s on the order of 10^9−10^{10} particles [Figure 2c(I)]. NPF due to non-thymol-based product F was associated with the largest number dose (mean $RTDD_N$ of 5.0 × 10^{10} particles), 10-fold larger than the dose associated with the thymol-based products (mean of B2, B3, and D1, 5.9 × 10^9 particles). The pulmonary region received the largest fraction of the total number dose (40−46%), followed by the tracheobronchial region and head airways. The high $RTDD_N$ in the pulmonary region is due to the high deposition fractions (DFs) for particles at D_a values from 20 to 50 nm in this region (Figure S28), which overlaps with the prominent mode of the SOA PN size distributions (Figure 1D). The number doses received during the indoor NPF events are equivalent to what one would receive when exposed to urban outdoor aerosols in a North American city for 30−100 min.[82] The SOA-forming potential of botanical disinfectants should be considered when evaluating the health risks associated with the indoor use of such products given the adverse toxicological effects associated with exposure to sub-100 nm SOA.[89−92]

The high PM_{10} mass concentrations of disinfectant droplets resulted in $RTDD_M$s from 10 to 28 μg [Figure 2c(II)]. Much of the mass dose was received in the head airways (63−75%) due to the high DFs of coarse mode particles in this region (Figure S28). While botanical disinfectants are commonly marketed as natural, green, and nontoxic alternatives to traditional chemical disinfectants, the multiphase exposures that they induce should not be overlooked and require further toxicological evaluation.

https://doi.org/10.1021/acs.estlett.1c00390
Environ. Sci. Technol. Lett. 2021, 8, 558−566

ASSOCIATED CONTENT

Supporting Information

The Supporting Information is available free of charge at https://pubs.acs.org/doi/10.1021/acs.estlett.1c00390.

A detailed description of the Purdue zEDGE Tiny House, the protocol for the botanical disinfectant emission experiments, a summary of the botanical disinfectant products, experimental conditions, operation and calibration of the PTR-TOF-MS, material balance model for determination of emission factors (EFs), calculation of inhalation intake fractions (iFs) and aerosol respiratory tract deposited doses (RTDDs), time series profiles for all 21 experiments across seven botanical disinfectants, a summary of identified VOCs and their properties, peak concentrations for VOCs and aerosols, and breathing rate-specific iFs and RTDDs (PDF)

AUTHOR INFORMATION

Corresponding Authors

Nusrat Jung − *Lyles School of Civil Engineering, Purdue University, West Lafayette, Indiana 47907, United States;* orcid.org/0000-0002-8874-8923; Email: nusratj@purdue.edu

Brandon E. Boor − *Lyles School of Civil Engineering and Ray W. Herrick Laboratories, Center for High Performance Buildings, Purdue University, West Lafayette, Indiana 47907, United States;* orcid.org/0000-0003-1011-4100; Email: bboor@purdue.edu

Authors

Jinglin Jiang − *Lyles School of Civil Engineering and Ray W. Herrick Laboratories, Center for High Performance Buildings, Purdue University, West Lafayette, Indiana 47907, United States;* orcid.org/0000-0001-6271-0436

Xiaosu Ding − *Lyles School of Civil Engineering, Purdue University, West Lafayette, Indiana 47907, United States;* orcid.org/0000-0003-2730-0823

Antonios Tasoglou − *RJ Lee Group Inc., Monroeville, Pennsylvania 15146, United States;* orcid.org/0000-0001-9767-5343

Heinz Huber − *Edelweiss Technology Solutions, LLC, Novelty, Ohio 44072, United States*

Amisha D. Shah − *Lyles School of Civil Engineering and Division of Environmental and Ecological Engineering, Purdue University, West Lafayette, Indiana 47907, United States;* orcid.org/0000-0003-0096-9922

Complete contact information is available at: https://pubs.acs.org/10.1021/acs.estlett.1c00390

Notes

The authors declare no competing financial interest.

ACKNOWLEDGMENTS

Financial support was provided by the Purdue University Office of the Executive Vice President for Research and Partnerships (Protect Purdue Innovations Faculty Grant to N.J., B.E.B., and A.D.S.) and the National Science Foundation (CBET-1847493 to B.E.B.). The authors are thankful for the help and support of Danielle N. Wagner and David Rater of the Lyles School of Civil Engineering at Purdue University.

REFERENCES

(1) Harvey, A. P.; Fuhrmeister, E. R.; Cantrell, M. E.; Pitol, A. K.; Swarthout, J. M.; Powers, J. E.; Nadimpalli, M. L.; Julian, T. R.; Pickering, A. J. Longitudinal Monitoring of SARS-CoV-2 RNA on High-Touch Surfaces in a Community Setting. *Environ. Sci. Technol. Lett.* **2021**, *8* (2), 168−175.

(2) Pitol, A. K.; Julian, T. R. Community Transmission of SARS-CoV-2 by Surfaces: Risks and Risk Reduction Strategies. *Environ. Sci. Technol. Lett.* **2021**, *8* (3), 263−269.

(3) Centers for Disease Control and Prevention (CDC). Guidance for Cleaning and Disinfecting Public Spaces, Workplaces, Businesses, Schools, and Homes. https://www.cdc.gov/coronavirus/2019-ncov/community/reopen-guidance.html (accessed 2021-01-20).

(4) U.S. Environmental Protection Agency (EPA). List N: Disinfectants for Coronavirus (COVID-19). 2020.

(5) Hora, P. I.; Pati, S. G.; McNamara, P. J.; Arnold, W. A. Increased Use of Quaternary Ammonium Compounds during the SARS-CoV-2 Pandemic and Beyond: Consideration of Environmental Implications. *Environ. Sci. Technol. Lett.* **2020**, *7* (9), 622−631.

(6) Zheng, G.; Filippelli, G. M.; Salamova, A. Increased Indoor Exposure to Commonly Used Disinfectants during the COVID-19 Pandemic. *Environ. Sci. Technol. Lett.* **2020**, *7* (10), 760−765.

(7) Wang, Z.; Kowal, S. F.; Carslaw, N.; Kahan, T. F. Photolysis-Driven Indoor Air Chemistry Following Cleaning of Hospital Wards. *Indoor Air* **2020**, *30* (6), 1241−1255.

(8) Mattila, J. M.; Arata, C.; Wang, C.; Katz, E. F.; Abeleira, A.; Zhou, Y.; Zhou, S.; Goldstein, A. H.; Abbatt, J. P. D.; Decarlo, P. F.; Farmer, D. K. Dark Chemistry during Bleach Cleaning Enhances Oxidation of Organics and Secondary Organic Aerosol Production Indoors. *Environ. Sci. Technol. Lett.* **2020**, *7* (11), 795−801.

(9) Matulonga, B.; Rava, M.; Siroux, V.; Bernard, A.; Dumas, O.; Pin, I.; Zock, J. P.; Nadif, R.; Leynaert, B.; Le Moual, N. Women Using Bleach for Home Cleaning Are at Increased Risk of Non-Allergic Asthma. *Respiratory Medicine* **2016**, *117*, 264−271.

(10) Nickmilder, M.; Carbonnelle, S.; Bernard, A. House Cleaning with Chlorine Bleach and the Risks of Allergic and Respiratory Diseases in Children. *Pediatric Allergy and Immunology* **2007**, *18* (1), 27−35.

(11) Zock, J. P.; Plana, E.; Antó, J. M.; Benke, G.; Blanc, P. D.; Carosso, A.; Dahlman-Höglund, A.; Heinrich, J.; Jarvis, D.; Kromhout, H.; Lillienberg, L.; Mirabelli, M. C.; Norbäck, D.; Olivieri, M.; Ponzio, M.; Radon, K.; Soon, A.; van Sprundel, M.; Sunyer, J.; Svanes, C.; Torén, K. Domestic Use of Hypochlorite Bleach, Atopic Sensitization, and Respiratory Symptoms in Adults. *J. Allergy Clin. Immunol.* **2009**, *124* (4), 731.

(12) Poppendieck, D.; Hubbard, H.; Corsi, R. L. Hydrogen Peroxide Vapor as an Indoor Disinfectant: Removal to Indoor Materials and Associated Emissions of Organic Compounds. *Environ. Sci. Technol. Lett.* **2021**, *8* (4), 320−325.

(13) Venu, S.; Naik, D. B.; Sarkar, S. K.; Aravind, U. K.; Nijamudheen, A.; Aravindakumar, C. T. Oxidation Reactions of Thymol: A Pulse Radiolysis and Theoretical Study. *J. Phys. Chem. A* **2013**, *117* (2), 291−299.

(14) Mastelić, J.; Jerković, I.; Blažević, I.; Poljak-Blaži, M.; Borović, S.; Ivančić-Baće, I.; Smrečki, V.; Žarković, N.; Brčić-Kostic, K.; Vikić-Topić, D.; Müller, N. Comparative Study on the Antioxidant and Biological Activities of Carvacrol, Thymol, and Eugenol Derivatives. *J. Agric. Food Chem.* **2008**, *56* (11), 3989−3996.

(15) Darpentigny, C.; Marcoux, P. R.; Menneteau, M.; Michel, B.; Ricoul, F.; Jean, B.; Bras, J.; Nonglaton, G. Antimicrobial Cellulose Nanofibril Porous Materials Obtained by Supercritical Impregnation of Thymol. *ACS Applied Bio Materials* **2020**, *3* (5), 2965−2975.

(16) Scaffaro, R.; Maio, A.; Nostro, A. Poly(Lactic Acid)/Carvacrol-Based Materials: Preparation, Physicochemical Properties, and Antimicrobial Activity. *Appl. Microbiol. Biotechnol.* **2020**, *104*, 1823−1835.

(17) Kang, J.; Song, K. B. Combined Washing Effect of Noni Extract and Oregano Essential Oil on the Decontamination of *Listeria*

Monocytogenes on Romaine Lettuce. *Int. J. Food Sci. Technol.* **2020**, *55* (11), 3515−3523.
(18) Hu, L.-B.; Ban, F.-F.; Li, H.-B.; Qian, P.-P.; Shen, Q.-S.; Zhao, Y.-Y.; Mo, H.-Z.; Zhou, X. Thymol Induces Conidial Apoptosis in Aspergillus Flavus via Stimulating K+ Eruption. *J. Agric. Food Chem.* **2018**, *66* (32), 8530−8536.
(19) Najafloo, R.; Behyari, M.; Imani, R.; Nour, S. A Mini-Review of Thymol Incorporated Materials: Applications in Antibacterial Wound Dressing. *J. Drug Delivery Sci. Technol.* **2020**, *60*, 101904.
(20) García-Salinas, S.; Gámez, E.; Asín, J.; de Miguel, R.; Andreu, V.; Sancho-Albero, M.; Mendoza, G.; Irusta, S.; Arruebo, M. Efficiency of Antimicrobial Electrospun Thymol-Loaded Polycaprolactone Mats in Vivo. *ACS Applied Bio Materials* **2020**, *3* (5), 3430−3439.
(21) van Noten, N.; van Liefferinge, E.; Degroote, J.; de Smet, S.; Desmet, T.; Michiels, J. Fate of Thymol and Its Monoglucosides in the Gastrointestinal Tract of Piglets. *ACS Omega* **2020**, *5* (10), 5241−5248.
(22) Kachur, K.; Suntres, Z. The Antibacterial Properties of Phenolic Isomers, Carvacrol and Thymol. *Crit. Rev. Food Sci. Nutr.* **2020**, *60*, 3042−3053.
(23) Zhou, W.; Wang, Z.; Mo, H.; Zhao, Y.; Li, H.; Zhang, H.; Hu, L.; Zhou, X. Thymol Mediates Bactericidal Activity against Staphylococcus Aureus by Targeting an Aldo-Keto Reductase and Consequent Depletion of NADPH. *J. Agric. Food Chem.* **2019**, *67*, 8382.
(24) Omonijo, F. A.; Liu, S.; Hui, Q.; Zhang, H.; Lahaye, L.; Bodin, J. C.; Gong, J.; Nyachoti, M.; Yang, C. Thymol Improves Barrier Function and Attenuates Inflammatory Responses in Porcine Intestinal Epithelial Cells during Lipopolysaccharide (LPS)-Induced Inflammation. *J. Agric. Food Chem.* **2019**, *67* (2), 615−624.
(25) Burgunter-Delamare, B.; Boyen, C.; Dittami, S. M. Effect of Essential Oil- and Iodine Treatments on the Bacterial Microbiota of the Brown Alga Ectocarpus Siliculosus. *J. Appl. Phycol.* **2021**, *33*, 459.
(26) Almasi, L.; Radi, M.; Amiri, S.; Torri, L. Fully Dilutable Thymus Vulgaris Essential Oil:Acetic or Propionic Acid Microemulsions Are Potent Fruit Disinfecting Solutions. *Food Chem.* **2021**, *343*, 128411.
(27) Liu, T.; Kang, J.; Liu, L. Thymol as a Critical Component of Thymus Vulgaris L. Essential Oil Combats Pseudomonas Aeruginosa by Intercalating DNA and Inactivating Biofilm. *LWT* **2021**, *136*, 110354.
(28) György, É.; Laslo, É.; Kuzman, I. H.; DezsöAndrás, C. The Effect of Essential Oils and Their Combinations on Bacteria from the Surface of Fresh Vegetables. *Food Sci. Nutr.* **2020**, *8* (10), 5601−5611.
(29) Wang, L.; Zhao, X.; Zhu, C.; Xia, X.; Qin, W.; Li, M.; Wang, T.; Chen, S.; Xu, Y.; Hang, B.; Sun, Y.; Jiang, J.; Richard, L. P.; Lei, L.; Zhang, G.; Hu, J. Thymol Kills Bacteria, Reduces Biofilm Formation, and Protects Mice against a Fatal Infection of Actinobacillus Pleuropneumoniae Strain L20. *Vet. Microbiol.* **2017**, *203*, 202−210.
(30) Meyers, C.; Robison, R.; Milici, J.; Alam, S.; Quillen, D.; Goldenberg, D.; Kass, R. Lowering the Transmission and Spread of Human Coronavirus. *J. Med. Virol.* **2021**, *93*, 1605.
(31) Sueishi, N.; Ohshima, T.; Oikawa, T.; Takemura, H.; Kasai, M.; Kitano, K.; Maeda, N.; Nakamura, Y. Plaque-Removal Effect of Ultrafine Bubble Water: Oral Application in Patients Undergoing Orthodontic Treatment. *Dent. Mater. J.* **2021**, *40*, 272.
(32) Angulo-Milhem, S.; Verriele, M.; Nicolas, M.; Thevenet, F. Indoor Use of Essential Oils: Emission Rates, Exposure Time and Impact on Air Quality. *Atmos. Environ.* **2021**, *244*, 117863.
(33) Chiu, H. H.; Chiang, H. M.; Lo, C. C.; Chen, C. Y.; Chiang, H. L. Constituents of Volatile Organic Compounds of Evaporating Essential Oil. *Atmos. Environ.* **2009**, *43* (36), 5743−5749.
(34) Nematollahi, N.; Kolev, S. D.; Steinemann, A. Volatile Chemical Emissions from Essential Oils. *Air Qual., Atmos. Health* **2018**, *11* (8), 949−954.
(35) Sarwar, G.; Corsi, R. The Effects of Ozone/Limonene Reactions on Indoor Secondary Organic Aerosols. *Atmos. Environ.* **2007**, *41* (5), 959−973.
(36) Coleman, B. K.; Lunden, M. M.; Destaillats, H.; Nazaroff, W. W. Secondary Organic Aerosol from Ozone-Initiated Reactions with Terpene-Rich Household Products. *Atmos. Environ.* **2008**, *42* (35), 8234−8245.
(37) Waring, M. S.; Wells, J. R.; Siegel, J. A. Secondary Organic Aerosol Formation from Ozone Reactions with Single Terpenoids and Terpenoid Mixtures. *Atmos. Environ.* **2011**, *45* (25), 4235−4242.
(38) Marjamäki, M.; Keskinen, J.; Chen, D. R.; Pui, D. Y. H. Performance Evaluation of the Electrical Low-Pressure Impactor (ELPI). *J. Aerosol Sci.* **2000**, *31* (2), 249−261.
(39) Marjamaki, M.; Lemmetty, M.; Keskinen, J. ELPI Response and Data Reduction I: Response Functions. *Aerosol Sci. Technol.* **2005**, *39* (7), 575−582.
(40) Lemmetty, M.; Keskinen, J.; Marjamäki, M. The ELPI Response and Data Reduction II: Properties of Kernels and Data Inversion. *Aerosol Sci. Technol.* **2005**, *39* (7), 583−595.
(41) Järvinen, A.; Aitomaa, M.; Rostedt, A.; Keskinen, J.; Yli-Ojanperä, J. Calibration of the New Electrical Low Pressure Impactor (ELPI+). *J. Aerosol Sci.* **2014**, *69*, 150−159.
(42) Saari, S.; Arffman, A.; Harra, J.; Rönkkö, T.; Keskinen, J. Performance Evaluation of the HR-ELPI+ Inversion. *Aerosol Sci. Technol.* **2018**, *52* (9), 1037−1047.
(43) Cappa, C. D.; Lovejoy, E. R.; Ravishankara, A. R. Determination of Evaporation Rates and Vapor Pressures of Very Low Volatility Compounds: A Study of the C4-C10 and C12 Dicarboxylic Acids. *J. Phys. Chem. A* **2007**, *111* (16), 3099−3109.
(44) Epstein, S. A.; Riipinen, I.; Donahue, N. M. A Semiempirical Correlation between Enthalpy of Vaporization and Saturation Concentration for Organic Aerosol. *Environ. Sci. Technol.* **2010**, *44* (2), 743−748.
(45) Nematollahi, N.; Kolev, S. D.; Steinemann, A. Volatile Chemical Emissions from Essential Oils. *Air Qual., Atmos. Health* **2018**, *11* (8), 949−954.
(46) Kokkini, S.; Karousou, R.; Lanaras, T. Essential Oils of Spearmint (Carvone-Rich) Plants from the Island of Crete (Greece). *Biochem. Syst. Ecol.* **1995**, *23* (4), 425−430.
(47) Msaada, K.; Hosni, K.; Taarit, M. B.; Chahed, T.; Kchouk, M. E.; Marzouk, B. Changes on Essential Oil Composition of Coriander (Coriandrum Sativum L.) Fruits during Three Stages of Maturity. *Food Chem.* **2007**, *102* (4), 1131−1134.
(48) Hoffmann, T.; Odum, J. R.; Bowman, F.; Collins, D.; Klockow, D.; Flagan, R. C.; Seinfeld, J. H. *J. Atmos. Chem.* **1997**, *26*, 189−222.
(49) Ehn, M.; Kleist, E.; Junninen, H.; Petäjä, T.; Lönn, G.; Schobesberger, S.; Dal Maso, M.; Trimborn, A.; Kulmala, M.; Worsnop, D. R.; Wahner, A.; Wildt, J.; Mentel, T. F. Gas Phase Formation of Extremely Oxidized Pinene Reaction Products in Chamber and Ambient Air. *Atmos. Chem. Phys.* **2012**, *12* (11), 5113−5127.
(50) Ehn, M.; Thornton, J. A.; Kleist, E.; Sipilä, M.; Junninen, H.; Pullinen, I.; Springer, M.; Rubach, F.; Tillmann, R.; Lee, B.; Lopez-Hilfiker, F.; Andres, S.; Acir, I. H.; Rissanen, M.; Jokinen, T.; Schobesberger, S.; Kangasluoma, J.; Kontkanen, J.; Nieminen, T.; Kurtén, T.; Nielsen, L. B.; Jørgensen, S.; Kjaergaard, H. G.; Canagaratna, M.; Maso, M. D.; Berndt, T.; Petäjä, T.; Wahner, A.; Kerminen, V. M.; Kulmala, M.; Worsnop, D. R.; Wildt, J.; Mentel, T. F. A Large Source of Low-Volatility Secondary Organic Aerosol. *Nature* **2014**, *506* (7489), 476−479.
(51) Jokinen, T.; Berndt, T.; Makkonen, R.; Kerminen, V. M.; Junninen, H.; Paasonen, P.; Stratmann, F.; Herrmann, H.; Guenther, A. B.; Worsnop, D. R.; Kulmala, M.; Ehn, M.; Sipilä, M. Production of Extremely Low Volatile Organic Compounds from Biogenic Emissions: Measured Yields and Atmospheric Implications. *Proc. Natl. Acad. Sci. U. S. A.* **2015**, *112* (23), 7123−7128.
(52) Chen, J.; Møller, K. H.; Wennberg, P. O.; Kjaergaard, H. G. Unimolecular Reactions Following Indoor and Outdoor Limonene Ozonolysis. *J. Phys. Chem. A* **2021**, *125* (2), 669−680.
(53) Youssefi, S.; Waring, M. S. Indoor Transient SOA Formation from Ozone+α-Pinene Reactions: Impacts of Air Exchange and Initial

Product Concentrations, and Comparison to Limonene Ozonolysis. *Atmos. Environ.* **2015**, *112*, 106−115.
(54) Nørgaard, A. W.; Kudal, J. D.; Kofoed-Sørensen, V.; Koponen, I. K.; Wolkoff, P. Ozone-Initiated VOC and Particle Emissions from a Cleaning Agent and an Air Freshener: Risk Assessment of Acute Airway Effects. *Environ. Int.* **2014**, *68*, 209−218.
(55) Friedman, B.; Farmer, D. K. SOA and Gas Phase Organic Acid Yields from the Sequential Photooxidation of Seven Monoterpenes. *Atmos. Environ.* **2018**, *187*, 335−345.
(56) Vartiainen, E.; Kulmala, M.; Ruuskanen, T. M.; Taipale, R.; Rinne, J.; Vehkamäki, H. Formation and Growth of Indoor Air Aerosol Particles as a Result of D-Limonene Oxidation. *Atmos. Environ.* **2006**, *40* (40), 7882−7892.
(57) Mehra, A.; Krechmer, J. E.; Lambe, A.; Sarkar, C.; Williams, L.; Khalaj, F.; Guenther, A.; Jayne, J.; Coe, H.; Worsnop, D.; Faiola, C.; Canagaratna, M. Oligomer and Highly Oxygenated Organic Molecule Formation from Oxidation of Oxygenated Monoterpenes Emitted by California Sage Plants. *Atmos. Chem. Phys.* **2020**, *20* (18), 10953−10965.
(58) Zhang, C.; Cao, X.; Sun, X.; Peng, H. Study on the Formation of Secondary Organic Aerosol by Ozonolysis of Citral in the Atmosphere. *Aerosol Air Qual. Res.* **2021**, *21*, 200637.
(59) Nunes, F. M. N.; Veloso, M. C. C.; Deppereira, P.; de Andrade, J. B. Gas-Phase Ozonolysis of the Monoterpenoids (S)-(+)-Carvone, (R)-(−)-Carvone, (−)-Carveol, Geraniol and Citral. *Atmos. Environ.* **2005**, *39* (40), 7715−7730.
(60) Bernard, F.; Daële, V.; Mellouki, A.; Sidebottom, H. Studies of the Gas Phase Reactions of Linalool, 6-Methyl-5-Hepten-2-Ol and 3-Methyl-1-Penten-3-Ol with O_3 and OH Radicals. *J. Phys. Chem. A* **2012**, *116* (24), 6113−6126.
(61) Sun, X.; Zhang, C.; Zhao, Y.; Bai, J.; He, M. Kinetic Study on the Linalool Ozonolysis Reaction in the Atmosphere. *Can. J. Chem.* **2012**, *90*, 353−361.
(62) Chen, X.; Hopke, P. K. A Chamber Study of Secondary Organic Aerosol Formation by Linalool Ozonolysis. *Atmos. Environ.* **2009**, *43* (25), 3935−3940.
(63) Li, M.; Weschler, C. J.; Bekö, G.; Wargocki, P.; Lucic, G.; Williams, J. Human Ammonia Emission Rates under Various Indoor Environmental Conditions. *Environ. Sci. Technol.* **2020**, *54* (9), 5419−5428.
(64) Na, K.; Song, C.; Switzer, C. R.; Cocker, D. Effect of Ammonia on Secondary Organic Aerosol Formation from α-Pinene Ozonolysis in Dry and Humid Conditions. *Environ. Sci. Technol.* **2007**, *41* (17), 6096−6102.
(65) Lehtipalo, K.; Yan, C.; Dada, L.; Bianchi, F.; Xiao, M.; Wagner, R.; Stolzenburg, D.; Ahonen, L. R.; Amorim, A.; Baccarini, A.; Bauer, P. S.; Baumgartner, B.; Bergen, A.; Bernhammer, A. K.; Breitenlechner, M.; Brilke, S.; Buchholz, A.; Mazon, S. B.; Chen, D.; Chen, X.; et al. Multicomponent New Particle Formation from Sulfuric Acid, Ammonia, and Biogenic Vapors. *Science Advances* **2018**, *4* (12), No. eaau5363.
(66) Kirkby, J.; Curtius, J.; Almeida, J.; Dunne, E.; Duplissy, J.; Ehrhart, S.; Franchin, A.; Gagné, S.; Ickes, L.; Kürten, A.; Kupc, A.; Metzger, A.; Riccobono, F.; Rondo, L.; Schobesberger, S.; Tsagkogeorgas, G.; Wimmer, D.; Amorim, A.; Bianchi, F.; Breitenlechner, M.; et al. Role of Sulphuric Acid, Ammonia and Galactic Cosmic Rays in Atmospheric Aerosol Nucleation. *Nature* **2011**, *476* (7361), 429−435.
(67) Almeida, J.; Schobesberger, S.; Kürten, A.; Ortega, I. K.; Kupiainen-Määttä, O.; Praplan, A. P.; Adamov, A.; Amorim, A.; Bianchi, F.; Breitenlechner, M.; David, A.; Dommen, J.; Donahue, N. M.; Downard, A.; Dunne, E.; Duplissy, J.; Ehrhart, S.; Flagan, R. C.; Franchin, A.; Guida, R.; et al. Molecular Understanding of Sulphuric Acid-Amine Particle Nucleation in the Atmosphere. *Nature* **2013**, *502* (7471), 359−363.
(68) Xiao, S.; Wang, M. Y.; Yao, L.; Kulmala, M.; Zhou, B.; Yang, X.; Chen, J. M.; Wang, D. F.; Fu, Q. Y.; Worsnop, D. R.; Wang, L. Strong Atmospheric New Particle Formation in Winter in Urban Shanghai, China. *Atmos. Chem. Phys.* **2015**, *15* (4), 1769−1781.
(69) Pryor, S. C.; Barthelmie, R. J.; Sørensen, L. L.; McGrath, J. G.; Hopke, P.; Petäjä, T. Spatial and Vertical Extent of Nucleation Events in the Midwestern USA: Insights from the Nucleation in ForesTs (NIFTy) Experiment. *Atmos. Chem. Phys.* **2011**, *11* (4), 1641−1657.
(70) Sihto, S. L.; Kulmala, M.; Kerminen, V. M.; Dal Maso, M.; Petäjä, T.; Riipinen, I.; Korhonen, H.; Arnold, F.; Janson, R.; Boy, M.; Laaksonen, A.; Lehtinen, K. E. J. Atmospheric Sulphuric Acid and Aerosol Formation: Implications from Atmospheric Measurements for Nucleation and Early Growth Mechanisms. *Atmos. Chem. Phys.* **2006**, *6* (12), 4079−4091.
(71) Nasr, G. G.; Whitehead, A.; Yule, A. J. Fine Sprays for Disinfection within Healthcare. *Int. J. Multiphys.* **2012**, *6* (2), 149−166.
(72) ASABE. ANSI/ASABE S572.3 Spray Nozzle Classification by Droplet Spectra. American Society of Agricultural and Biological Engineers: St. Joseph, MI, 2020.
(73) Li, X.; Shang, Y.; Yan, Y.; Yang, L.; Tu, J. Modelling of Evaporation of Cough Droplets in Inhomogeneous Humidity Fields Using the Multi-Component Eulerian-Lagrangian Approach. *Building and Environment* **2018**, *128*, 68−76.
(74) Bai, C.; Gosman, A. D. Development of Methodology for Spray Impingement Simulation. In *SAE Technical Papers*; SAE International, 1995. DOI: 10.4271/950283
(75) Quadros, M. E.; Marr, L. C. Silver Nanoparticles and Total Aerosols Emitted by Nanotechnology-Related Consumer Spray Products. *Environ. Sci. Technol.* **2011**, *45*, 10713−10719.
(76) SB 258, Lara. Cleaning Product Right to Know Act of 2017. 2017.
(77) Bennett, D. H.; McKone, T. E.; Evans, J. S.; Nazaroff, W. W.; Margni, M. D.; Jolliet, O.; Smith, K. R. Peer Reviewed: Defining Intake Fraction. *Environ. Sci. Technol.* **2002**, *36* (9), 206A−211A.
(78) Nazaroff, W. W. Inhalation Intake Fraction of Pollutants from Episodic Indoor Emissions. *Building and Environment* **2008**, *43* (3), 269−277.
(79) Jolliet, O.; Ernstoff, A. S.; Csiszar, S. A.; Fantke, P. Defining Product Intake Fraction to Quantify and Compare Exposure to Consumer Products. *Environ. Sci. Technol.* **2015**, *49* (15), 8924−8931.
(80) Hussein, T.; Boor, B. E.; Löndahl, J. Regional Inhaled Deposited Dose of Indoor Combustion-Generated Aerosols in Jordanian Urban Homes. *Atmosphere* **2020**, *11*, 1150.
(81) Hussein, T.; Löndahl, J.; Paasonen, P.; Koivisto, A. J.; Petäjä, T.; Hämeri, K.; Kulmala, M. Modeling Regional Deposited Dose of Submicron Aerosol Particles. *Sci. Total Environ.* **2013**, *458−460*, 140−149.
(82) Wu, T.; Boor, B. Urban Aerosol Size Distributions: A Global Perspective. *Atmos. Chem. Phys. Discuss.* **2020**, 1−83.
(83) Anjilvel, S. A Multiple-Path Model of Particle Deposition in the Rat Lung. *Fundam. Appl. Toxicol.* **1995**, *28* (1), 41−50.
(84) Miller, F. J.; Asgharian, B.; Schroeter, J. D.; Price, O. Improvements and Additions to the Multiple Path Particle Dosimetry Model. *J. Aerosol Sci.* **2016**, *99*, 14−26.
(85) National Institute for Public Health and the Environment (RIVM). Multiple Path Particle Dosimetry Model (MPPD v 1.0): A Model for Human and Rat Airway Particle Dosimetry. RIVA Report 650010030; RIVA: Bilthoven, The Netherlands, 2002.
(86) U.S. Environmental Protection Agency (EPA). *Exposure Factors Handbook: 2011 edition*; EPA: Washington, DC, 2011.
(87) Yao, M.; Weschler, C. J.; Zhao, B.; Zhang, L.; Ma, R. Breathing-Rate Adjusted Population Exposure to Ozone and Its Oxidation Products in 333 Cities in China. *Environ. Int.* **2020**, *138*, 105617.
(88) Lai, A. C. K.; Thatcher, T. L.; Nazaroff, W. W. Inhalation Transfer Factors for Air Pollution Health Risk Assessment. *J. Air Waste Manage. Assoc.* **2000**, *50* (9), 1688−1699.
(89) Oberdörster, G. Pulmonary Effects of Inhaled Ultrafine Particles. *Int. Arch. Occup. Environ. Health* **2000**, *74*, 1−8.
(90) Oberdörster, G.; Sharp, Z.; Atudorei, V.; Elder, A.; Gelein, R.; Kreyling, W.; Cox, C. Translocation of Inhaled Ultrafine Particles to the Brain. *Inhalation Toxicol.* **2004**, *16* (6−7), 437−445.

https://doi.org/10.1021/acs.estlett.1c00390
Environ. Sci. Technol. Lett. 2021, 8, 558−566

(91) Elder, A.; Oberdörster, G. Translocation and Effects of Ultrafine Particles Outside of the Lung. *Clinics in Occupational and Environmental Medicine* **2006**, 5 (4), 785−96.
(92) Lin, Y. H.; Arashiro, M.; Martin, E.; Chen, Y.; Zhang, Z.; Sexton, K. G.; Gold, A.; Jaspers, I.; Fry, R. C.; Surratt, J. D. Isoprene-Derived Secondary Organic Aerosol Induces the Expression of Oxidative Stress Response Genes in Human Lung Cells. *Environ. Sci. Technol. Lett.* **2016**, 3 (6), 250−254.